JETIR.ORG ISSN: 2349-5162 | ESTD Year : 2014 | Monthly Issue
JOURNAL OF EMERGING TECHNOLOGIES AND INNOVATIVE RESEARCH (JETIR)
An International Scholarly Open Access, Peer-reviewed, Refereed Journal

Crosslinking-Dependent Swelling, Diffusion and Mechanical Behavior of Thermoresponsive Hydrogels

Rashmi Kumari[a], Varun Kumar Singh[b], Suman Shekhar[c*]

[a]Jagjiwan College, Gaya Ji (Magadh University, Bodhgaya, Bihar) India 823003

[b]Teerthanker Mahaveer University, Moradabad, Uttar Pradesh 244001, India

[c*]Daudnagar College, Daudnagar, Aurangabad (Magadh University, Bodhgaya (Bihar), India 824113

Abstract

This study systematically investigates the effect of crosslinking ratio on the network structure, swelling and mechanical properties of poly (NIPAM-co-NTBA-co-AAm) hydrogels. Equilibrium swelling data were used to calculate the average molecular mass between crosslinks (Mc) and polymer–solvent interaction parameter (χ). Increasing crosslinking ratio enhanced crosslink density, decreased Mc and reduced equilibrium swelling. Diffusion studies showed Fickian transport for NTA1 and NTA2, while NTA3–NTA5 followed non-Fickian behavior. Short- and long-time swelling kinetics were analyzed using the power law, Berens–Hopfenberg and Schott's models. Average diffusion coefficients declined with higher crosslinking, consistent with restricted chain mobility. The χ parameter decreased with reduced MBA content, confirming conventional crosslinking effects. Mechanical studies revealed that higher crosslinking ratios increased elastic and shear moduli as well as compressive resistance, reflecting stronger, stiffer networks. Overall findings demonstrate that crosslinking ratio strongly governs hydrogel swelling, diffusion and mechanical performance.

Key Words: NIPAM, swelling kinetics, network parameters, crosslink density.

1. Introduction

Poly(N-isopropylacrylamide) (PNIPAM)-based thermoresponsive hydrogels are among the most extensively studied crosslinked polymers due to their unique ability to absorb and retain large amounts of water within their three-dimensional networks [1–3]. Owing to their remarkable swelling properties, these hydrogels have emerged as promising candidates for diverse biomedical applications, including controlled drug delivery

systems, artificial implants, dialysis membranes, burn dressings and cardiovascular devices [4–6]. Since the performance of such applications critically depends on the swelling capacity of the hydrogel, a fundamental understanding of the swelling behavior and water–polymer interactions is essential [7–9]. In addition to providing maximum swelling and water-retention capacity, swelling studies also offer valuable insights into the network structure in the hydrated state as well as the diffusion mechanisms governing water absorption [9–13]. While high swelling capacity typically enhances permeability and biocompatibility, it may also compromise the mechanical stability of the hydrogel, presenting a trade-off that must be addressed.

Over the past three decades, a wide range of studies have reported the physicochemical characteristics of NIPAM-based copolymeric hydrogels, such as equilibrium swelling, polymer–solvent interactions, elasticity and swelling/shrinking kinetics [14–17]. However, their relatively low swelling capacity and poor mechanical strength have restricted their applicability. Achieving the simultaneous combination of high swelling and robust mechanical performance remains a crucial challenge for both industrial and biomedical uses [18,19]. To overcome these limitations, researchers have explored various chemical modification strategies, including altering the concentration and type of crosslinking agents, adjusting synthesis methods, designing hydrophobically modified copolymers, incorporating nanocomposite reinforcements, developing double-network systems and introducing hydrophilic comonomers to tune swelling behavior and adjust the lower critical solution temperature (LCST) [1,2,9–11,19,20]. For instance, Caykara et al. examined the influence of N,N′-methylenebis(acrylamide) (MBAAm) content on the LCST, network architecture and swelling properties of PNIPAM [21], while Mah and co-workers investigated how crosslinker concentration governs the swelling ratio and polymer–water interaction parameter [19]. More recently, Hoti et al. (2021) elucidated the correlation between cross-linking density and the swelling/mechanical behavior of cyclodextrin-based nanosponges using Flory–Rehner theory and rheology [22]. Similarly, Kenari et al. (2018) highlighted the effects of cross-linker chain length on the rheological and swelling characteristics of dextran hydrogels [23].

The structural and elastic properties of hydrogels are strongly influenced by the concentration and chemical nature of the crosslinking agent as well as the molecular weight between crosslinks (Mc). Cross-linking density plays a decisive role in determining swelling behavior and mechanical strength, which are key factors in tailoring NIPAM-based hydrogels for specific applications [22,24–25]. Mc, in particular, is a critical parameter that governs the volume phase transition and overall mechanical response of the hydrogel.

In our earlier work, we reported the synthesis and characterization of poly(NIPAM-co-NTBA-co-AAm) hydrogels for the separation of aqueous protein solutions [14]. Building upon this foundation, the present study investigates the influence of crosslinker concentration on the network structure, swelling kinetics and mechanical strength of poly(NIPAM-co-NTBA-co-AAm) hydrogels. To the best of our knowledge, a systematic study evaluating the effects of cross-linking ratio on swelling, mechanical performance and crosslinking density in these hydrogels has not yet been reported. Here, we employ Flory–Rehner theory and compression testing to evaluate key network parameters, including molecular weight between cross-links (Mc), crosslinking density (Ve), elastic modulus (E) and compression modulus (G). Furthermore, we analyze the

thermodynamics of swelling to provide deeper insights into structure–property correlations. This study introduces a novel perspective in the PNIPAM-based hydrogel literature by presenting, for the first time, a systematic investigation of the impact of cross-linking density on the physicochemical properties of poly(NIPAM-co-NTBA-co-AAm).

2. Experimental

2.1 Materials

N-isopropylacrylamide (NIPAM), *N-tert-butylacrylamide* (NTBA) and acrylamide (AAm) monomers were procured from TCI (Tokyo Chemical Industry, USA). N,N′-methylenebis(acrylamide) (MBA) was employed as a crosslinking agent, ammonium persulfate (APS) as an initiator and N,N,N′,N′-tetramethylethylenediamine (TEMED) as an accelerator; all were purchased from Central Drug House Ltd. Co. (CDH, India). Additionally, 1,4-dioxane (CDH, India) was used as a co-solvent during hydrogel synthesis. Analytical reagent (AR) grade chemicals were used throughout and double-distilled water was employed in all swelling and deswelling experiments.

2.2 Hydrogel Preparation

Random copolymers of NIPAM, NTBA and AAm with varying compositions were synthesized via free radical polymerization, following a modified procedure reported earlier [14]. To obtain hydrogels with different swelling capacities, the total molar amounts of NIPAM, NTBA and AAm were kept constant, while the molar ratio of MBA was systematically varied.

The detailed feed compositions used for preparing poly(NIPAM-co-NTBA-co-AAm) hydrogels are summarized in **Table 1**.

Table 1: The different proportions of monomers and reagents in copolymer composition

NIPAM/NTBA/ AAm (Molar ratio)	MBA (moles) $\times 10^{-8}$	APS (moles) $\times 10^{-4}$	TEMED (20 vol %)	Nomenclature
25/37.5/37.5	0.00649	1.85	0.25	NTA1
25/37.5/37.5	0.0194	1.85	0.25	NTA2
25/37.5/37.5	0.0779	1.85	0.25	NTA3
25/37.5/37.5	0.155	1.85	0.25	NTA4
25/37.5/37.5	0.233	1.85	0.25	NTA5

2.3 Characterizations

The structural and morphological characteristics of the poly(NIPAM-co-NTBA-co-AAm) hydrogels were analyzed using multiple techniques. Fourier transform infrared (FTIR) spectra were recorded with a Shimadzu IR Prestige-21 spectrometer (Japan) in diffuse reflectance spectroscopy (DRS) mode to confirm functional group incorporation. The surface morphology of vacuum-dried gels was examined using scanning electron microscopy (SEM; JSM-6390LV, Jeol, Japan) at magnifications up to 10,000×, after sputter-coating the cut surfaces with gold for 30 min using a JSC-1600 coater. Mechanical behavior was investigated by uniaxial

compression testing with a Universal Testing Machine (Instron 3360), where samples were pre-equilibrated in deionized water at 25 °C for 48 h and vacuum grease was applied to minimize dehydration during testing; compressive stress (F′/A) was measured at a constant deformation rate of 1 mm/min with three replicates per group. Swelling experiments were performed by immersing dried hydrogel samples in distilled water at different temperatures using a constant-temperature water bath until equilibrium was reached.

3. Results and Discussion

3.1 Fourier Transform Infrared spectroscopy (FTIR)

The FTIR spectra of the synthesized poly(NIPAM-co-NTBA-co-AAm) hydrogels (Figure 1) verify the successful copolymerization of the monomers into a stable terpolymer network. A broad absorption in the range of 3100–3547 cm^{-1} corresponds to N–H stretching, while the distinct peak at 1649 cm^{-1} is characteristic of amide C=O stretching vibrations. The signal at 1612 cm^{-1} is associated with the asymmetric stretching of carboxylate groups and the band at 1448 cm^{-1} represents their symmetric stretching. A notable band at 1532 cm^{-1} arises from N–H bending of the amide linkage, further supporting the incorporation of acrylamide moieties. Additionally, the band at 2129 cm^{-1} can be attributed to –C–N stretching, originating from the crosslinker N,N′-methylene bisacrylamide in combination with the copolymer backbone. The iso-intensity doublet peaks at 1394 and 1353 cm^{-1} correspond to the symmetrical bending and splitting vibrations of the dimethyl groups in isopropyl units, whereas the absorption at 1224 cm^{-1} indicates the presence of a tert-butyl group ($–C(CH_3)_3$) from NTBA. Collectively, these spectral assignments confirm the incorporation of NIPAM, NTBA and AAm segments within the polymer matrix, thereby validating the formation of the desired hydrogel network [9, 10, 14–17].

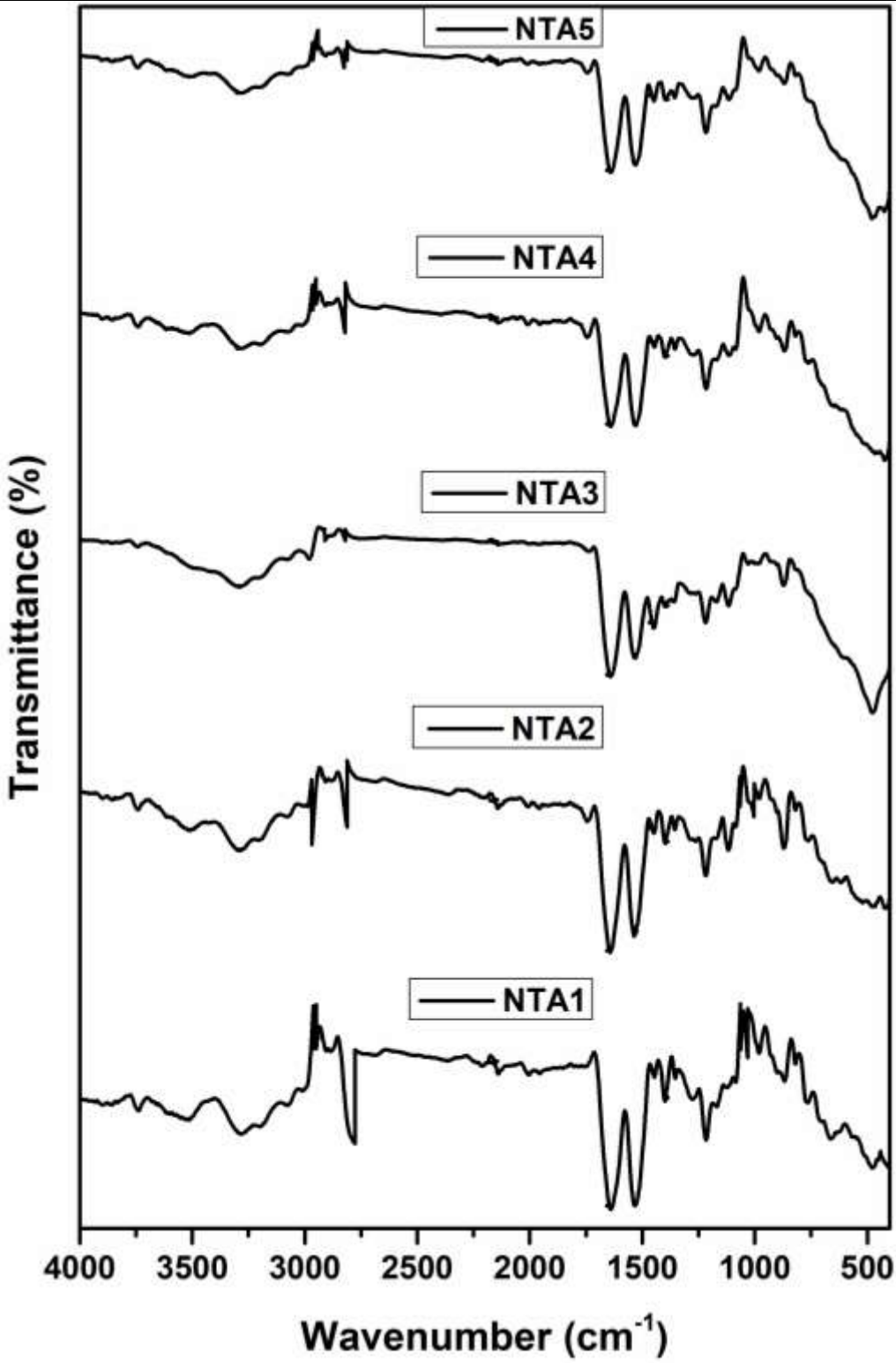

Fig. 1. FTIR spectra of the NTA hydrogels of different crosslinking ratio.

3.2 Microscopic study

The SEM micrographs in Figure 2 show the surface morphology of dried hydrogels NTA1, NTA2, NTA3, NTA4 and NTA5.

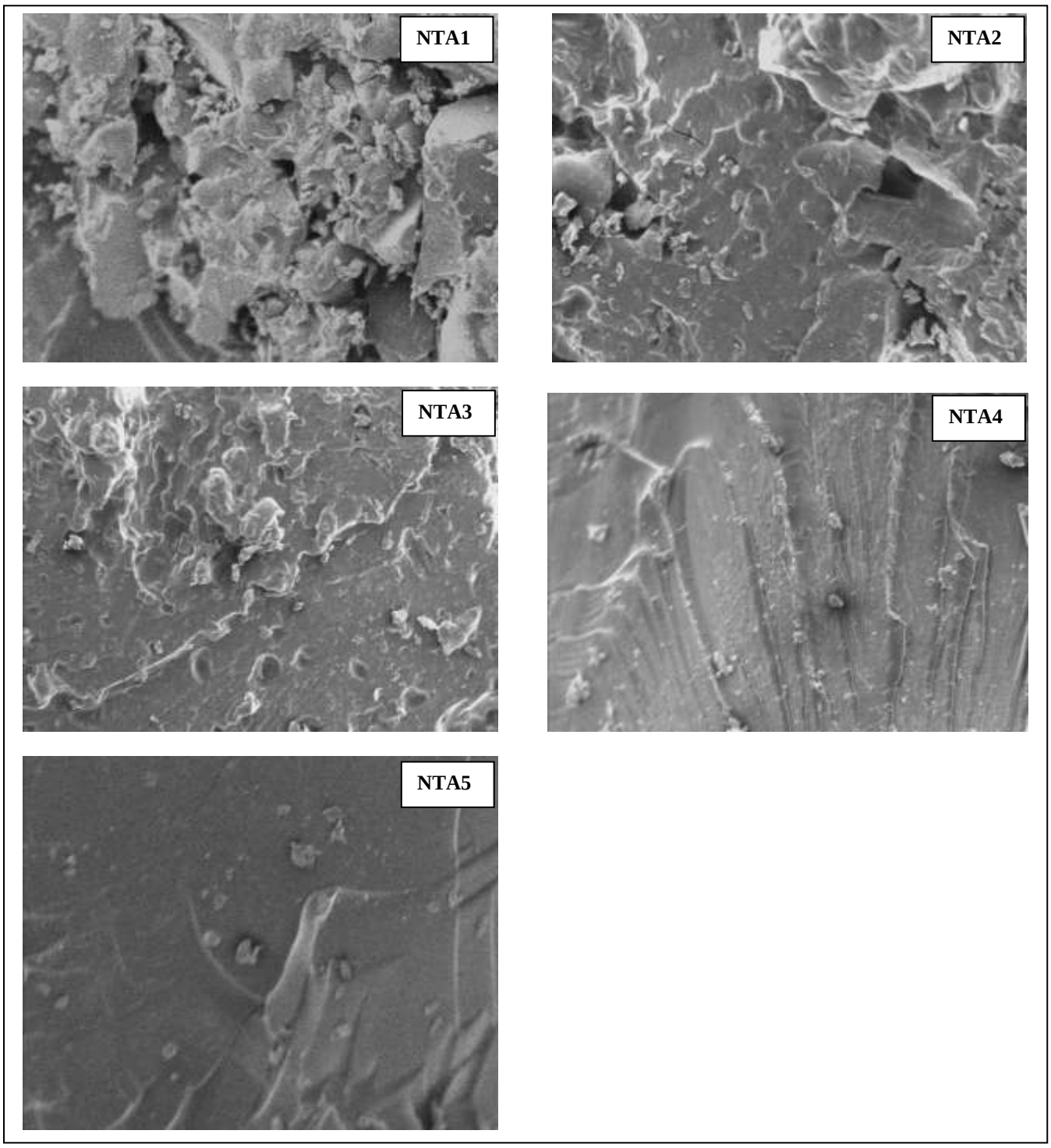

Figure 2 SEM image of dried NTA1, NTA2, NTA3, NTA4 and NTA5 hydrogels

The surface morphology of the poly(NIPAM-co-NTBA-co-AAm) hydrogels, as examined by SEM, clearly demonstrates the influence of crosslinking density on the structural features of the network. Hydrogels prepared with a higher concentration of crosslinker exhibited relatively smooth, dense and compact surfaces. This compactness can be attributed to the stronger intermolecular interactions among polymer chains, which promote the formation of a tightly bound three-dimensional network. Such enhanced connectivity between

chains reduces the availability of free volume and voids, thereby imparting a more uniform and compact appearance in the dried state. In contrast, hydrogels synthesized with lower crosslinking ratios displayed heterogeneous and irregular surface morphologies. The reduced degree of crosslinking likely results in weaker chain-to-chain interactions and the presence of larger interstitial spaces within the polymer matrix. Upon drying, these loosely packed regions collapse unevenly, giving rise to surface discontinuities, pores, or cracks. This observation suggests that the crosslinking ratio plays a pivotal role in governing the morphological stability of the hydrogels, with higher crosslinking yielding structurally robust and compact networks, whereas lower crosslinking favors irregular architectures with poor mechanical integrity [14].

3.3 Determination of Network Parameter of the hydrogels

The swelling properties of hydrogels are significantly influenced by the hydrophilic–hydrophobic balance of the polymer network, the presence of ionizable groups and most importantly, the degree of crosslinking [14–17, 26]. Among these, the average molecular weight between crosslinks (Mc) is a critical parameter, as it directly controls the crosslink density, swelling ratio, mechanical strength and the volume phase transition behavior of the gel. The Flory–Rehner theory offers a well-established thermodynamic framework to describe swelling, where equilibrium is achieved through a balance between the osmotic driving force of polymer–solvent mixing and the elastic retractive forces of the network [27–29]. In this model, M_c and related parameters such as crosslink density (V_e) are derived from measurable swelling data using the Flory–Huggins polymer–solvent interaction parameter (χ) and solvent molar volume. This theoretical treatment not only explains the equilibrium swelling phenomenon but also provides a quantitative tool for predicting and optimizing the network architecture of hydrogels [30–34].

To determine the network parameters, five hydrogel samples with different crosslinking ratios were subjected to swelling studies in distilled water at 25 °C. The change in mass of each sample was recorded at regular time intervals until equilibrium swelling was achieved.

Table 2 Network and swelling parameters of hydrogels with varying crosslinking ratio

Samples	Crosslinking ratio($\times 10^{-3}$)	Average molecular mass between crosslinks (M_c) (kg/mole)	Theoretical M_c(kg)	Crosslink density ($\times 10^{-3}$)	Elastically effective chains V_e ($\times 10^{18}$)
NTA1	1.6	155.27	33.51	0.69	2.80
NTA2	4.8	149.31	11.17	0.72	3.31
NTA3	19.4	39.09	2.79	2.7	13.96
NTA4	38.9	6.58	1.39	16.52	86.70
NTA5	58.4	1.47	0.93	73.88	409.05

During the swelling of polymeric hydrogels, the entropy of mixing between solvent molecules and polymer chains generates an osmotic driving force that facilitates water uptake into the network. At the same time,

stretching of the polymer chains reduces their configurational entropy, giving rise to an elastic restoring force that counteracts swelling. Equilibrium swelling is attained when these two opposing contributions are balanced [30, 35–37]. According to the Flory–Rehner model, the affinity of water for the hydrophilic polymer chains is expressed through the mixing term of the free energy $\ln(1-\phi)$, ϕ and $\chi\phi^2$, whereas the elastic term $[V_s \times (V_e/V_0) \times (\phi^{1/3} - \phi/2)]$ represents the resistance due to network stretching [38, 39].

Network parameters of hydrogels prepared with varying crosslinking ratios. The data include molecular weight between crosslinks (M_c), number of elastically effective chains per unit volume (V_e) and Flory–Huggins interaction parameter (χ). A decrease in M_c with increasing crosslinker content indicates denser network structures, leading to reduced swelling. Conversely, higher Mc values correspond to loosely crosslinked networks with greater swelling capacity. The experimental M_c values are consistently higher than the theoretical predictions (M_{ct}), reflecting deviations from ideal Gaussian network behavior [40-42]. A slight increase in χ with higher crosslinking ratio is attributed to the lower hydrophilicity of MBAAm

3.4 Swelling and deswelling kinetics

The dried hydrogel samples with varying crosslinking ratios were subjected to swelling studies at different temperatures (5, 25, 50 and 60°C) and the corresponding swelling kinetics are illustrated in Figure 3. As anticipated, both the swelling rate and the equilibrium swelling ratio declined progressively with increasing crosslinking content. This behavior can be attributed to the reduction in free volume and pore size of the network as the crosslinking density increases, thereby restricting the diffusion of water molecules into the polymer matrix. From a morphological perspective, hydrogels with a lower degree of crosslinking exhibit larger discontinuities between polymer domains, which facilitate rapid water uptake. In contrast, higher crosslinking ratios promote the aggregation of polymer chains into compact domains, often forming microspherical or spherical structures. Such compact domain arrangements hinder the penetration of water, thereby lowering both the rate of swelling and the overall equilibrium swelling capacity.

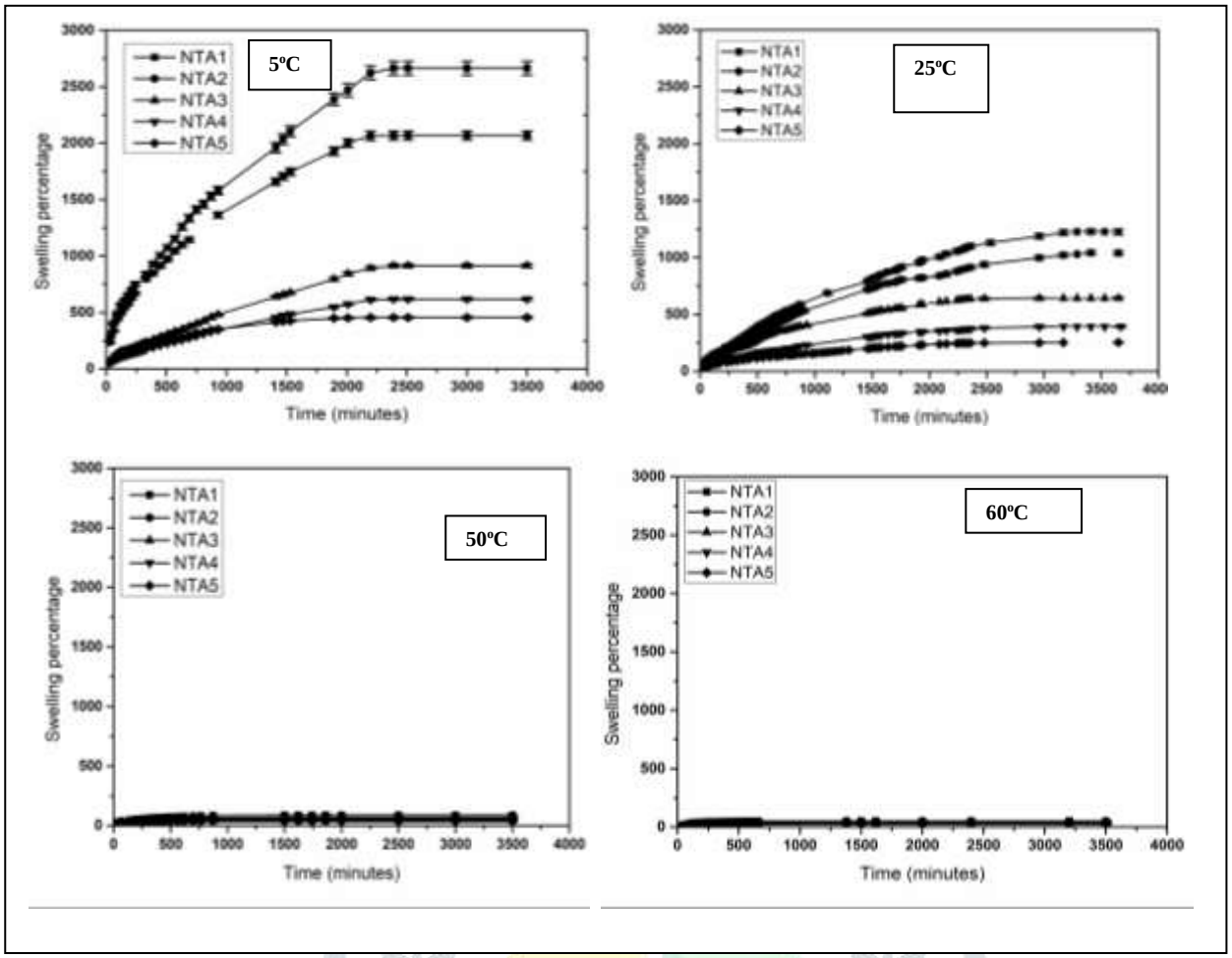

Figure 3: Swelling percentage of NTA1, NTA2, NTA3, NTA4 and NTA5 at 5, 25, 50 and 60°C

To investigate the effect of crosslinking ratio on the water diffusion behavior in the hydrogels, the initial swelling data were analyzed using the power-law equation [26, 42]:

$$F = \frac{M_t}{M_\infty} = kt^n \qquad (1)$$

Where F is the fractional water uptake at time‘t’, M_t is the mass of water absorbed at time t and M_∞ is equilibrium water uptake, k is the gel characteristic constant related to the network structure and n is the swelling exponent characterizing the diffusion mechanism. For cylindrical hydrogel samples, values of n between 0.45–0.5 correspond to Fickian diffusion, while 0.5<n<1 indicates non-Fickian or anomalous transport [43].

The initial stage of swelling for the poly(NIPAM-co-NTBA-co-AAm) hydrogels was fitted to Equation 1 and ln(F) versus ln(t) was plotted to determine the diffusion behavior (Figure 4). The slope and intercept of these plots were used to calculate the swelling exponent n and gel constant k, respectively. The calculated values are summarized in Table 3, providing quantitative insight into the influence of crosslinking density on the water transport mechanism within the hydrogel networks.

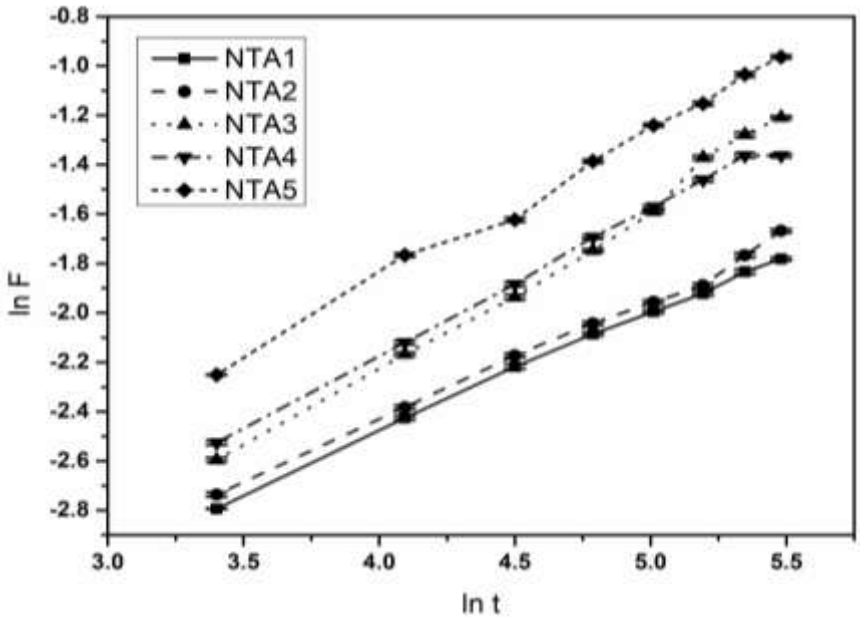

Figure 4: Diffusion kinetics of NTA1, NTA2, NTA3, NTA4 and NTA5 copolymers

The calculated values of the swelling exponent (n), as summarized in Table 3, fall within the range of 0–1, confirming that the water transport behavior in these hydrogels is governed by both Fickian and non-Fickian mechanisms. Specifically, the hydrogels designated as NTA1 and NTA2 exhibit n values close to 0.5, indicating Fickian diffusion, where the rate of water penetration is slower than the relaxation rate of polymer chains. In contrast, the hydrogels NTA3, NTA4 and NTA5 demonstrate n values between 0.5 and 1, corresponding to anomalous or non-Fickian diffusion. This suggests that in these formulations, the rates of solvent penetration and polymer chain relaxation are comparable, leading to a coupled diffusion–relaxation process. Such findings highlight the critical role of crosslinking density in dictating the diffusion mechanism, where lower crosslinking favors simple Fickian transport, while higher crosslinking introduces complexities associated with network rigidity and polymer–solvent interactions.

The swelling exponent (n) values for NTA3, NTA4 and NTA5 are 0.68, 0.58 and 0.61, respectively, indicating anomalous or non-Fickian diffusion. This behavior suggests that the rates of water diffusion and polymer chain relaxation are comparable, with swelling increasingly governed by chain relaxation rather than solvent penetration. Additionally, a gradual increase in n from NTA1 to NTA5 highlights a transition from Fickian to non-Fickian transport as the crosslinking ratio increases. This trend can be attributed to the higher crosslinking density, which restricts network mobility and emphasizes chain-relaxation-controlled swelling. These observations confirm that crosslinking density is a key factor in modulating the water transport mechanism within the hydrogels network.

Table 3 Kinetic parameters of NTA1, NTA2, NTA3, NTA4 and NTA5 copolymers

	Power law equation			Berens hopfenberg equation			Schott's equation		
	k	n	R^2	A	k_1	R^2	A	B	R^2
NTA1	0.01213	0.48	0.99	-1.22	0.00115	0.99	117.86	0.1306	0.98
NTA2	0.01209	0.49	0.99	-1.08	0.00118	0.98	205.4	0.147	0.96
NTA3	0.00712	0.68	0.99	-0.88	0.00115	0.97	220.0	0.369	0.99
NTA4	0.01115	0.58	0.99	-0.87	0.0006	0.98	419.0	0.64	0.98
NTA5	0.01308	0.61	0.99	-0.84	0.0007	0.98	367.0	1.12	0.99

While the power-law (Peppas) equation provides a reliable description of the initial swelling behavior, it is less accurate for fractional water uptake above $M_t/M_\infty = 0.60$. To better model the diffusion behavior during the later stages of swelling, Berens and Hopfenberg proposed a differential approach that accounts for extended swelling times and higher solvent penetration [21]:

This model allows for a more precise characterization of water transport in hydrogels beyond the initial 60% of equilibrium swelling, capturing both diffusion and polymer relaxation effects over prolonged periods.

$$\frac{dM_t}{dt} = k_1(M_\infty - M_t) \quad (2)$$

$$\frac{M_t}{M_\infty} = 1 - Aexp(-k_1 t) \quad (3)$$

In the Berens–Hopfenberg model, k_1 (min^{-1}) represents the relaxation rate constant and A is a model-specific constant. These parameters were determined by fitting the entire swelling dataset beyond $M_t/M_\infty=0.60$ to the linearized form of the equation, ln (1- M_t/M_∞) versus time (t) (Figure 5). The slope of this plot provides k_1, while the intercept yields A, allowing for a more accurate description of the hydrogel swelling kinetics at later stages, where the power-law approach becomes less precise.

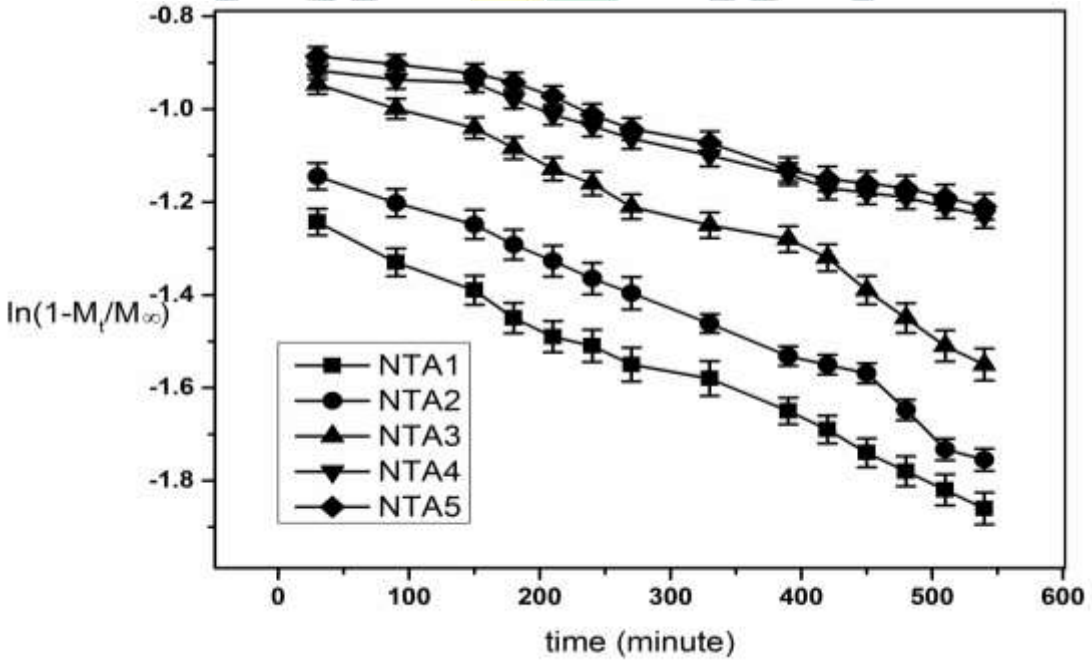

Figure 5: Plots of ln (1- M_t/M_∞) versus time t for NTA1, NTA2, NTA3, NTA4 and NTA5 copolymers

The values of A and k_1 obtained from the Berens–Hopfenberg analysis are summarized in Table 3, where it is evident that A increases with higher crosslinking ratios.

For hydrogels subjected to longer swelling periods, the overall kinetics can be more accurately described using Schott's second-order swelling model [26, 43]:

$$\frac{t}{M_t} = A + Bt \quad (4)$$

where M_t represents the water uptakes at time t and A and B are two characteristics coefficients. At longer times, as equilibrium swelling is approached Bt >> A, Equation (4) simplifies to slop B = $1/M_\infty$, indicating that B is the reciprocal of the equilibrium swelling capacity [26, 43]. Conversely, at very short swelling times A>> Bt and in the limit, Eq. (4) becomes

$$\lim_{t\to 0} \frac{dM_t}{dt} = \frac{1}{A} \quad (5)$$

This shows that the intercept A corresponds to the reciprocal of the initial swelling rate. This model therefore provides a more comprehensive representation of hydrogels swelling kinetics over the entire swelling period, from the initial uptake to equilibrium. [26, 43].

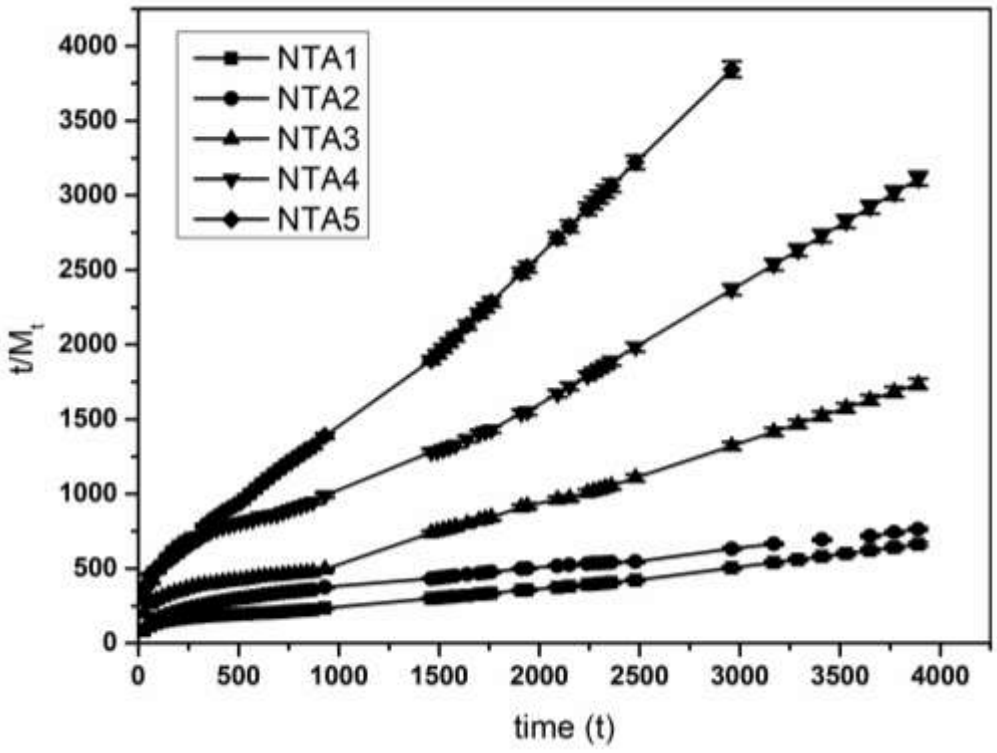

Figure 6: Plots of t/M_t versus time t for NTA1, NTA2, NTA3, NTA4 and NTA5 copolymers

The plots of t/M_t vs t are presented in Figure 6 and the corresponding values of constants A and B are summarized in Table 3. All hydrogel samples exhibited excellent correlation coefficients, with the plots showing nearly linear trends and only slight deviations at the initial stages. This observation confirms that the swelling behavior of the hydrogels follows second-order kinetics, where the long-term swelling process is predominantly governed by polymer chain relaxation rather than diffusion [43]. Similar findings have also been reported in earlier studies [44, 45].

The deswelling kinetics of NTA1, NTA2, NTA3, NTA4 and NTA5 hydrogels were investigated gravimetrically at 60°C, with water retention measured at different time intervals (Figure 7). The results show that all hydrogels exhibited nearly identical deswelling rates and water retention profiles. This behavior can be attributed to the comparable hydrophilic–hydrophobic balance in their network structures, suggesting that variations in crosslinking ratio have minimal influence on the deswelling characteristics under the studied conditions.

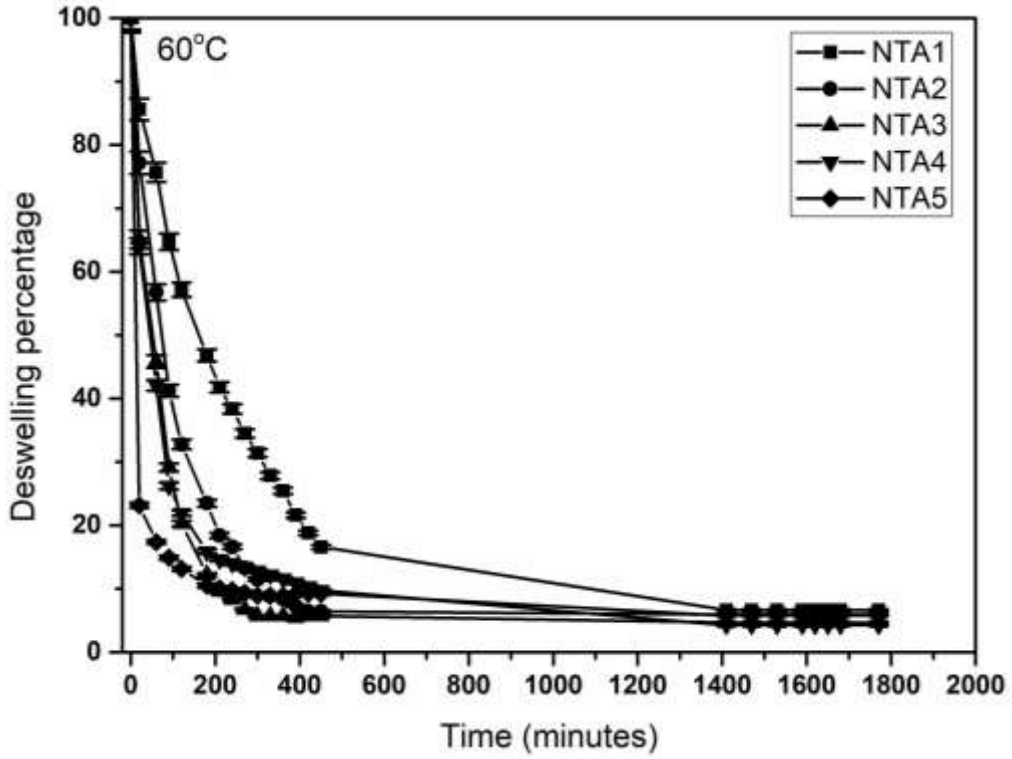

Figure 7: Water retention for NTA1, NTA2, NTA3, NTA4 and NTA5 copolymers at 60°C

3.5 Diffusion Coefficient

It is well established that a Fickian diffusion curve is characterized by a smooth, monotonic and inflection-free progression towards equilibrium, whereas case II transport typically produces a distinctly sigmoidal profile [46]. To differentiate between these two mechanisms, the swelling data at 25 °C were analyzed by plotting M_t/M_∞ as functions of $t^{1/2}$, as shown in Figure 8. The resulting curves display a sigmoidal nature, suggesting that the water uptake process in the hydrogels is more consistent with case II transport rather than purely Fickian diffusion. Nevertheless, after the initial lag phase ($t^{1/2} < 15$, corresponding to $M_t/M_\infty < 0.38$), the swelling profiles in the range of ($0.07 < M_t/M_\infty < 0.38$) exhibit an approximately linear relationship. The slopes of these linear regions were subsequently employed to calculate the initial diffusion coefficients using the following relation:

$$\frac{M_t}{M_\infty} = F = 4[(Dt/\pi l^2)^{\frac{1}{2}}]` \quad (6)$$

where D is the diffusion coefficient and l is average thickness of the cylindrical sample.

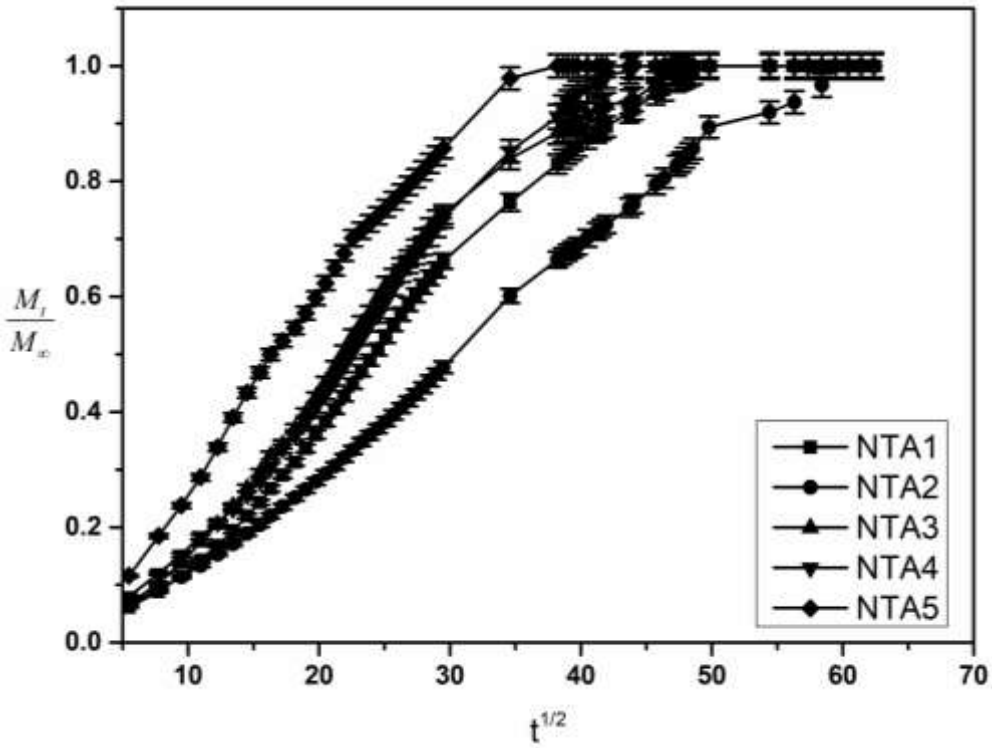

Figure 8: Plots of M_t/M_∞ versus time $t^{1/2}$ for NTA1, NTA2, NTA3, NTA4 and NTA5 copolymers

In the case of cylindrical hydrogel geometries, the diffusion coefficients typically fall within the order of 10^{-7} [47]. However, in the present investigation, the calculated diffusion coefficients were found to be relatively higher. This observation suggests an accelerated ingress of solvent molecules into the hydrogel matrix, which can be attributed to the structural features of the prepared networks. The increased diffusion may arise from the presence of more accessible free volume within the polymer network or a favorable hydrophilic–hydrophobic balance, which facilitates rapid water transport. Such deviations from the commonly reported values further support the non-Fickian diffusion mechanism discussed earlier, where both solvent penetration and polymer chain relaxation play significant roles in controlling the swelling kinetics.

Table 4 $D_{initial}$, D_L, D_{avg} and activation energy of NTA1, NTA2, NTA3, NTA4 and NTA5 copolymers

	Diffusion coefficient (initial)	D_L	D_{Avg}	Activation energy	R^2
NTA1	0.00014889	2.26927E-05	7.368E-05	13.65333	0.87
NTA2	0.00013953	1.69875E-05	6.657E-05	12.37359	0.92
NTA3	0.00012518	1.57603E-05	6.324E-05	14.24334	0.98
NTA4	0.00010997	1.12433E-05	5.499E-05	15.09096	0.93
NTA5	9.3471E-05	9.00594E-06	5.421E-05	14.89152	0.98

Diffusion coefficients can also be calculated using the late-time approximation [48]:

$$\frac{M_t}{M_\infty} = 1 - 8\left[8/\pi^2\left\{\exp\left(-\left(\frac{\pi^2 Dt}{4l^2}\right)\right)\right\}\right] \quad (7)$$

Using the data for last 60% swelling, plots for ln (1- $\frac{M_t}{M_\infty}$) versus t are drawn and with the slope of the linear plots thus obtained, late-time diffusion coefficient D_L may be calculated using the following expression:

$$D_L = -(\text{Slope} \times l^2/\pi^2) \quad (8)$$

The average diffusion coefficient D_{avg} was calculated for 50% of the total water uptake by putting F =0.5 in the equation 30 which finally yield following equation [49]:

$$D_{avg}=0.049\, l^2/t_{1/2} \quad (9)$$

Where $t_{1/2}$ is the time required for 50% of equilibrium swelling.

All the three types of diffusion coefficients calculated—initial diffusion coefficient, average diffusion coefficient and late-time diffusion coefficient are summarized in Table 4. A closer examination of these values reveals some interesting insights. It is evident that all three diffusion coefficients decrease progressively with increasing crosslinking ratio of the hydrogels. This trend can be explained by the fact that hydrogels with lower crosslinking density possess more flexible chains and greater free volume, allowing enhanced chain relaxation during the swelling process. Consequently, water molecules can diffuse more rapidly into the polymer network, leading to higher diffusion coefficients at lower crosslinking ratios [26, 43, 49].

Furthermore, it is consistently observed that for each hydrogels, the initial diffusion coefficient is greater than both the average and late-time diffusion coefficient. This behavior is attributed to the faster water uptake in the initial stages, when abundant free hydrophilic sites are available for interaction with water molecules. As swelling progresses, however, the diffusion rate slows down due to increased resistance from the already hydrated polymer chains and decreased availability of free sites. Thus, the diffusion kinetics exhibits a characteristic transition from rapid initial uptake to a slower, relaxation-controlled process at longer times.

3.6 Effect of temperature on water uptake, diffusion and interaction parameter

The swelling behavior of thermoresponsive hydrogels is strongly influenced by the temperature of the swelling medium, primarily due to the sharp volume phase transition occurring around the lower critical solution temperature (LCST). In the present study, the effect of temperature on the water uptake of hydrogel samples was investigated over the range of 5–60°C in distilled water (Figure 9). The results indicate that equilibrium swelling decreases with increasing temperature. This can be attributed to enhanced hydrophobic interactions among polymer chains at elevated temperatures, which reduce the availability of hydrophilic domains for water uptake, thereby confirming the thermoresponsive nature of the hydrogels. Furthermore, at all studied temperatures, the equilibrium swelling percentage was consistently higher for hydrogels with lower crosslinking ratios, reflecting their more open network structure and greater capacity for water absorption.

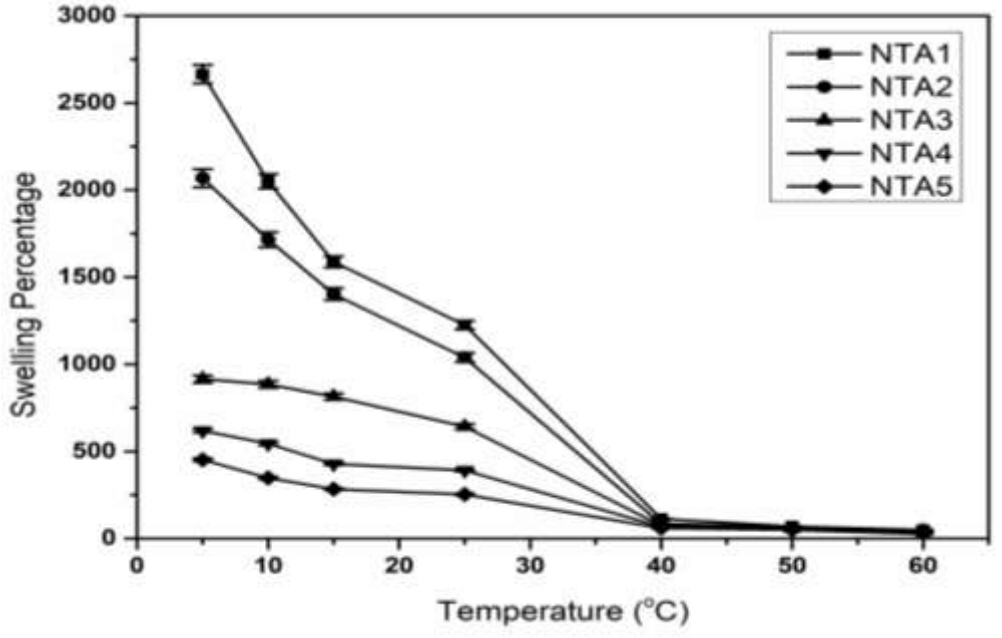

Figure 9: Equilibrium swelling percentage of NTA1, NTA2, NTA3, NTA4 and NTA5 at 5, 10, 15, 25, 40, 50 and 60°C

The diffusion coefficients of the hydrogels were observed to increase with rising temperature (Figure 10). This trend can be explained by the thermoresponsive nature of the polymer networks, where elevated temperatures enhance the molecular mobility of water and polymer chains, thereby facilitating faster solvent transport. The apparent increase in diffusion may also be linked to the reduced water retention capacity of the hydrogels at higher temperatures, leading to relatively quicker penetration of solvent molecules into the network. To further quantify this temperature dependence, the variation of diffusion coefficients with temperature was analyzed using an Arrhenius-type relationship [47].

$$D = D_o \exp(E_D/RT) \quad (10)$$

In this context, E_D represents the apparent activation energy governing the diffusion process. The relationship between the logarithm of the diffusion coefficient (D) and the reciprocal of temperature ($1/T_1$) is presented in Figure 11, demonstrating a linear trend consistent with Arrhenius behavior. From the slopes of these plots, the activation energies for NTA1, NTA2, NTA3, NTA4 and NTA5 hydrogels were calculated and are summarized in Table 4.

Interestingly, the average activation energy obtained for the cylindrical hydrogels in the present study is 14.05 kJ mol^{-1}, which is considerably higher than the reported value of 8.3 kJ $mol^{-1}$for non-ionic cylindrical hydrogels [50]. This elevated energy requirement suggests that the water diffusion in our hydrogel system is comparatively slower. Such behavior aligns well with the predictions of the Tanaka–Fillmore theory, which emphasizes the dominant role of polymer chain relaxation in controlling swelling kinetics [51].

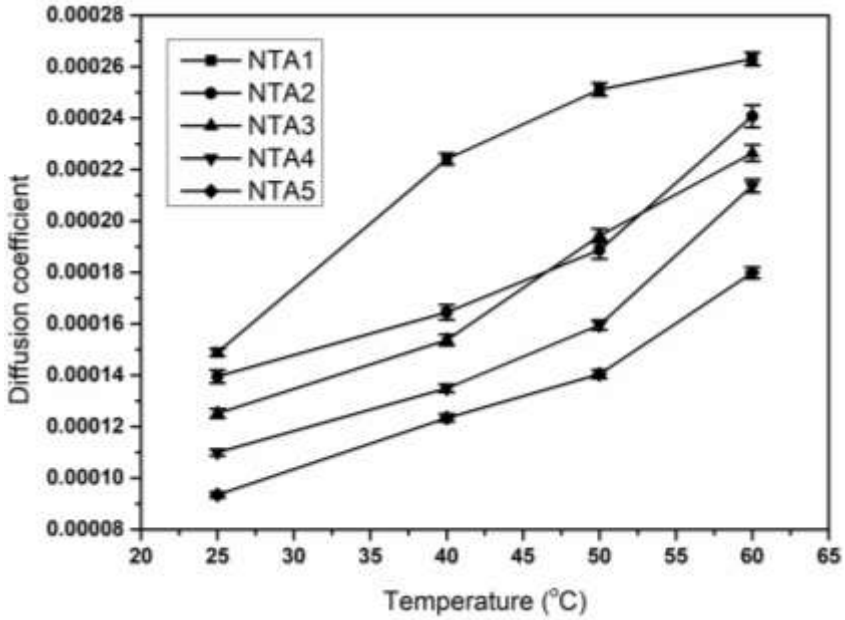

Figure 10: Plots of D versus temperature for NTA1, NTA2, NTA3, NTA4 and NTA5 copolymers

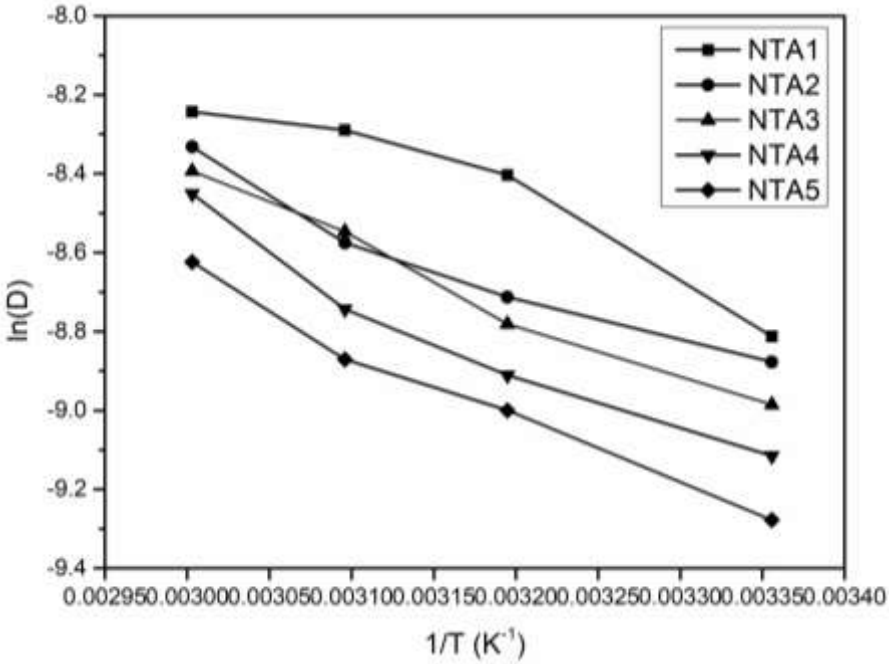

Figure 11: Plots of ln(D) versus 1/T for NTA1, NTA2, NTA3, NTA4 and NTA5 copolymers

The enthalpy of mixing (ΔH_{mix}) between the dry polymer and an infinite amount of water was evaluated for the hydrogel samples NTA1, NTA2, NTA3, NTA4 and NTA5. This parameter was determined by measuring the maximum water uptake of the hydrogels within the temperature range of 5–60 °C. The calculations were carried out using the Gibbs–Helmholtz equation, which establishes the relationship between the free energy of mixing, enthalpy and temperature [47].

$$\frac{d\ lnM_{\infty}}{d(\frac{1}{T})} = \frac{\Delta H_{mix}}{R} \quad (11)$$

where R is the gas constant and T is the temperature on absolute scale.

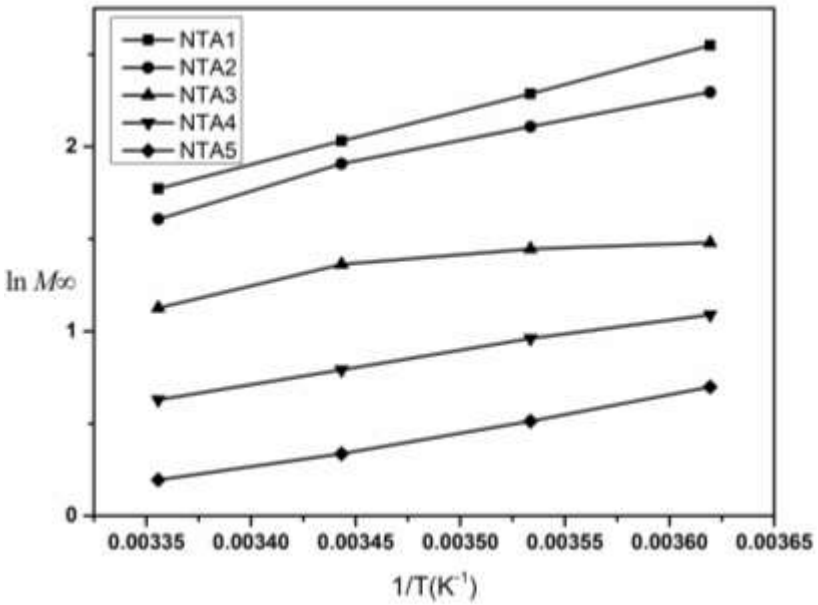

Figure 12: Plots of ln M∞ versus 1/T for NTA1, NTA2, NTA3, NTA4 and NTA5 copolymers

Figure 12 shows the plots of ln M_∞ and 1/T for all hydrogel samples, which yielded straight lines with positive slopes. From these plots, the enthalpies of mixing were calculated as 26.62, 23.77, 15.91, 14.23 and 12.48 kJ mol^{-1} for NTA1, NTA2, NTA3, NTA4 and NTA5, respectively. The negative sign of enthalpy values indicates that the swelling process is endothermic in nature. Moreover, the relatively lower values of ΔH_{mix} correspond to higher swelling capacities of the hydrogels, as less energy is required to promote polymer–solvent interactions.

As illustrated in Figure 13, the polymer–solvent interaction parameter (χ) increases with rising temperature. This trend can be attributed to the reduced water absorption capacity of the hydrogel network at elevated temperatures. The decrease in water uptake is a consequence of the hydrophilic-to-hydrophobic transition of the polymer chains as the solution temperature exceeds the lower critical solution temperature (LCST). Below the LCST, the amide groups of NIPAM, NTBA and AAm are capable of forming hydrogen bonds with water molecules, facilitating strong water retention within the network. However, as temperature increases beyond the LCST, the hydrophobic hydration process dominates, leading to the expulsion of water molecules from the network. This release of bound water molecules is accompanied by an increase in the overall entropy of the polymer–water system, thereby making the deswelling process spontaneous. Thus, the thermoresponsive behavior of the hydrogels above their LCST is primarily governed by the balance between hydrogen bonding interactions and hydrophobic hydration [52].

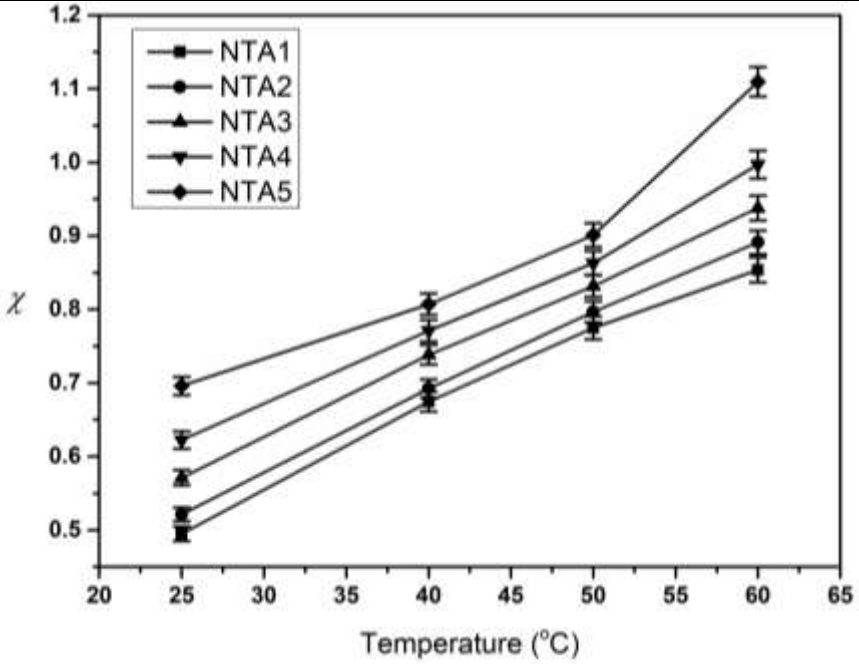

Figure 13: Plots of χ vs temperature for NTA1, NTA2, NTA3, NTA4 and NTA5 copolymers

The temperature-dependent swelling behavior of NTA1, NTA2, NTA3, NTA4 and NTA5 hydrogels was further interpreted using the **Flory–Rehner theory of swelling equilibrium**. According to this theory, the osmotic pressure (π) of a non-ionic hydrogel system arises from two distinct contributions: (i) the osmotic pressure generated by polymer–solvent mixing (π_{mix}) and (ii) the elastic restoring force (π_{ei}) that develops due to deformation of the polymer network chains into an elongated configuration [28]. The osmotic contribution from polymer–solvent mixing can be described using the Flory–Huggins model as:

$$\pi_{mix} = -\frac{RT}{V_1}(\ln(1 - v_2) + v_2 + \chi {v_2}^2) \qquad (12)$$

where R is the universal gas constant, T is the absolute temperature, V_1 is the molar volume of the solvent, v_2 is the polymer volume fraction in the swollen state and χ is the Flory–Huggins interaction parameter that characterizes polymer–solvent affinity. The interaction parameter χ is not constant but depends on polymer concentration and temperature. It can be expressed as a power series expansion in terms of v_2 [45];

$$\chi = \chi_1 + \chi_2 v_2 + \chi_3 {v_2}^2 + \ldots\ldots \qquad (13)$$

where χ_1, χ_2, χ_3……..are empirical coefficients that depend on both the molecular nature of the polymer–solvent system and temperature [45]. For hydrogels exhibiting large degrees of swelling**,** the polymer volume fraction v_2 becomes very small and higher-order terms can be neglected. Under this condition, χ reduces primarily to its first term χ_1,, which is given by the thermodynamic relation [28]

$$\chi_1 = \frac{\Delta G}{RT} = \frac{\Delta H - T\Delta S}{RT} \qquad (14)$$

Here, ΔG, ΔH and ΔS correspond to the changes in free energy, enthalpy and entropy, respectively, associated with replacing polymer–polymer and solvent–solvent contacts by polymer–solvent contacts [45].

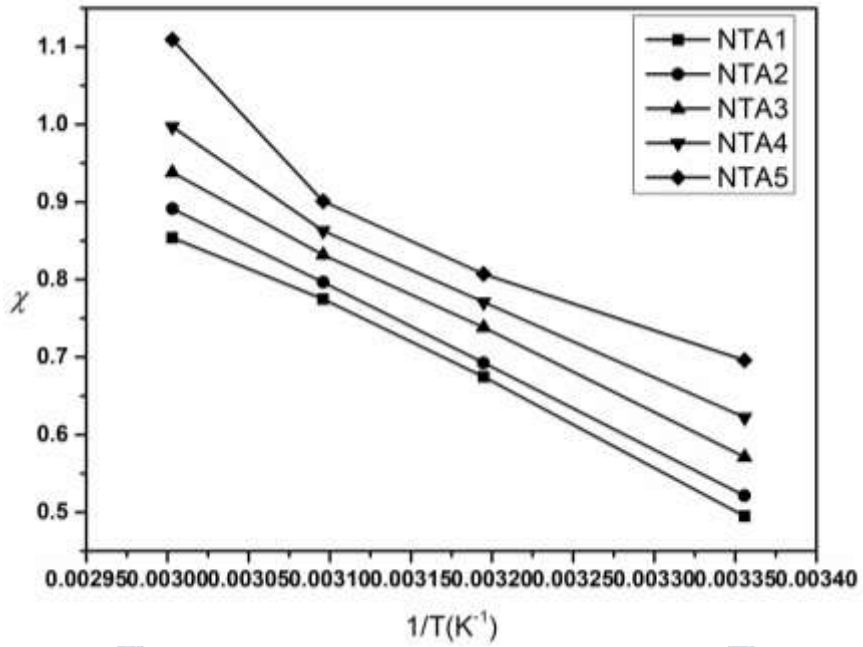

Figure 14: Plots of χ vs 1/T for NTA1, NTA2, NTA3, NTA4 and NTA5 copolymers

The interaction parameters χ plotted as function of 1/T (Figure 14) which are found to be linear indicating that the enthalpy and the entropy contributions to the interaction parameter are constant and χ equals to χ_1 in this range of concentration and temperature (Equation 14). The slope and the intercept at 1/T=0 of these lines give the ΔH and ΔS values (Equation 14).

The results of ΔH and ΔS are displayed in Table 5. It is seen that the signs of both quantities are negative for all the hydrogels. Since polymer–solvent systems possessing the LCST are characterized by negative values of both ΔH and ΔS, the results indicate that all the NTA hydrogels studied in the present work have LCST's. Moreover, the absolute values of both ΔH and ΔS increase with increasing amount of crosslinker MBA indicating that the thermoresponsive properties of the hydrogels increase with increasing crosslinking ratio [45]. The variation of the Flory–Huggins interaction parameter (χ) with reciprocal temperature (1/T) is illustrated in Figure 14**.** The linear dependence of χ on 1/T indicates that the enthalpic (ΔH) and entropic (ΔS) contributions to χ remain constant within the studied concentration and temperature range. Under these conditions, χ effectively reduces to χ_1 as described in Equation (14). From the slope and intercept of the χ vs. 1/T plots, the values of ΔH and ΔS were determined (Table 5). The calculated results clearly demonstrate that both ΔH and ΔS are negative for all hydrogel formulations. This observation is in excellent agreement with the theoretical prediction that polymer–solvent systems exhibiting a lower critical solution temperature (LCST) typically display negative enthalpy and entropy values. The negative ΔH reflects the endothermic nature of water–polymer interactions, while the negative ΔS arises from the reduction in configurational freedom of water molecules bound to the polymer chains below the LCST. Furthermore, the magnitudes of ΔH and ΔS were found to increase with increasing concentration of the crosslinker (MBA). This suggests that the introduction of additional crosslinking points enhances the thermoresponsive nature of the hydrogels. In other words, hydrogels with higher crosslinking ratios exhibit more pronounced phase transition behavior across the LCST, which is

attributed to stronger hydrophilic–hydrophobic balance and more cooperative structural rearrangements during swelling–deswelling cycles [45].

Table 5 Enthalpy and entropy changes appearing in the χ parameter for the of NTA1, NTA2, NTA3, NTA4 and NTA5 copolymers

Samples	ΔH (J/mole)	ΔS (J/moleK)	ΔG
NTA1	-8523.2	-32.7665	1208.452
NTA2	-8731.34	-33.6402	1259.8
NTA3	-8818.91	-33.9133	1253.332
NTA4	-9037.17	-34.8545	1314.627
NTA5	-9244.01	-36.5322	1606.046

3.7 Swelling and compression measurements

Cylindrical hydrogel samples with dimensions of 1.0 cm height and 0.8 cm diameter were equilibrated in water at 25 °C to attain swelling equilibrium. Under the assumption of isotropic swelling, the swelling ratio can be expressed as the reciprocal of the polymer volume fraction according to Equation (15):

$$\frac{V_s}{V_r} = \frac{\vartheta_{2r}}{\vartheta_{2s}} = \left(\frac{d}{d_o}\right)^3 \qquad (15)$$

where ϑ_{2s} and ϑ_{2r} represent the polymer volume fractions in the relaxed and swollen states, respectively. These parameters can be calculated using the following relations:

$$\vartheta_{2r} = C_o\left(\frac{M_o}{\rho_2}\right) \qquad (16)$$

$$\vartheta_{2s} = \vartheta_{2r}\left(\frac{d_o}{d}\right)^3 \qquad (17)$$

Where, C_o is the initial monomer concentration, ρ_2 is the density of the dry polymer and M_o is the molecular weight of repeat unit of the hydrogel.

The mechanical properties of the hydrogels were analyzed in terms of Young's modulus (E) and shear modulus (G). The compressive stress (τ) was related to strain using the following equations:

$$.\tau = E\ (\lambda - 1) \qquad (18)$$

$$\tau = G(\lambda - \lambda^{-2}) \qquad (19)$$

where λ is the deformation ratio, defined as the deformed length divided by the initial length of the sample. From the slope of the linear portion of the τ versus $(\lambda - \lambda^{-2})$ plots the shear modulus (G) was obtained, which was further used to estimate the effective crosslinking density V_e through the Flory–Rehner approach: [53]

$$V_e = \frac{G}{RTV_{2s}^{\frac{1}{3}}V_{2r}^{\frac{2}{3}}} \qquad (20)$$

After getting the values of V_e, ϑ_{2r} and ϑ_{2s} the polymer–water interaction parameter, χ can be calculated from Flory–Rehner equilibrium swelling equation [26–28].

$$\chi = \frac{-\left[ln(1-\vartheta_{2s}) + \vartheta_{2s} + V_e V_1 \vartheta_{2r}\left\{\left(\vartheta_{2s}/\vartheta_{2r}\right)^{1/3} - \left(\vartheta_{2s}/\vartheta_{2r}\right)\left(\frac{1}{2}\right)\right\}\right]}{\vartheta_{2s}^{\,2}} \qquad (21)$$

To investigate the influence of structural parameters and crosslinking ratio on the mechanical behavior of NTA1–NTA5 hydrogels, compressive stress–strain and stress–linear deformation factor plots were constructed (Figures 15–18). The slopes of the linear regions of these plots were used to determine the elastic modulus (E) and shear modulus (G) using Equations (40) and (41), respectively (Table 6). Subsequently, the shear modulus values, together with the polymer volume fractions in equilibrium (V_{2s}) and relaxed states (V_{2r}) states, were employed in Equation (42) to evaluate the polymer–water interaction parameter (χ) (Table 6).

The results revealed that strain percentage increased with increasing crosslinking ratio, highlighting the enhanced compressibility of the NTA hydrogels (NTA1–NTA5) with higher MBA content. As shown in Table 6, NTA5 hydrogels with the highest crosslinker concentration exhibited superior mechanical strength and higher elastic modulus compared with other formulations. A progressive increase in both E and G with increasing crosslinking ratio confirmed the reinforcement of mechanical strength with denser crosslinking networks [54,55]. Comparable findings have also been reported in previous studies [20,22,53].

Furthermore, the polymer–water interaction parameter (χ) displayed a decreasing trend with higher crosslinking density, consistent with conventional crosslinking processes (Table 6). This suggests that tighter network structures restrict solvent–polymer interactions, thereby lowering χ values and further enhancing the structural stability of the hydrogels.

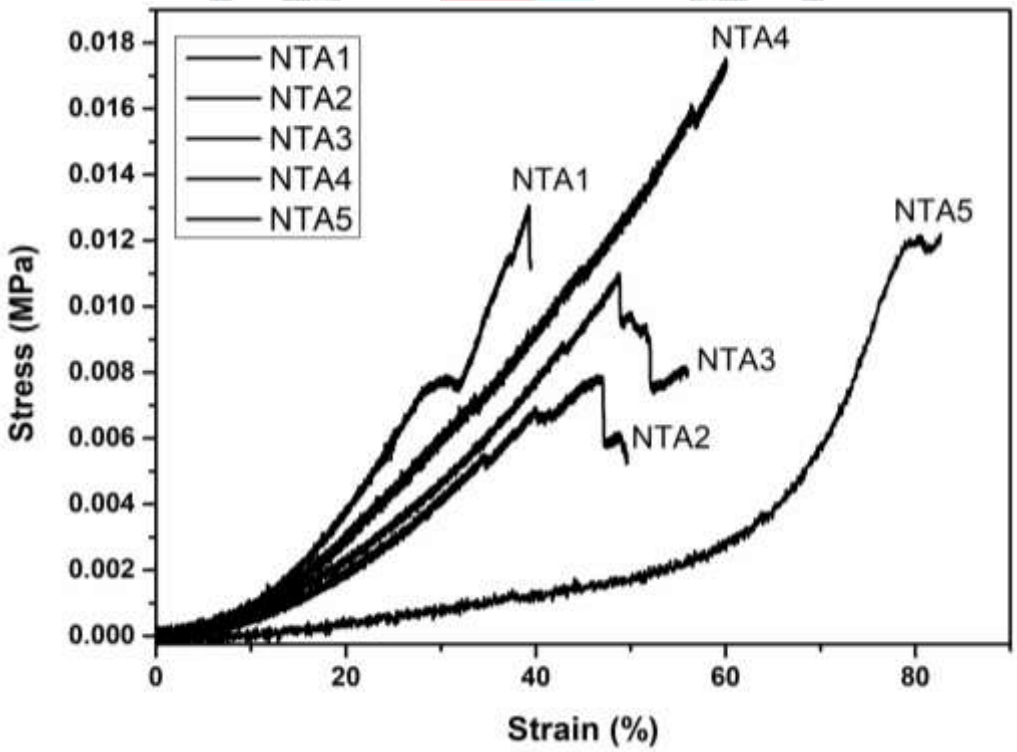

Figure 15: Plots of Stress vs strain for NTA1, NTA2, NTA3, NTA4 and NTA5 copolymers

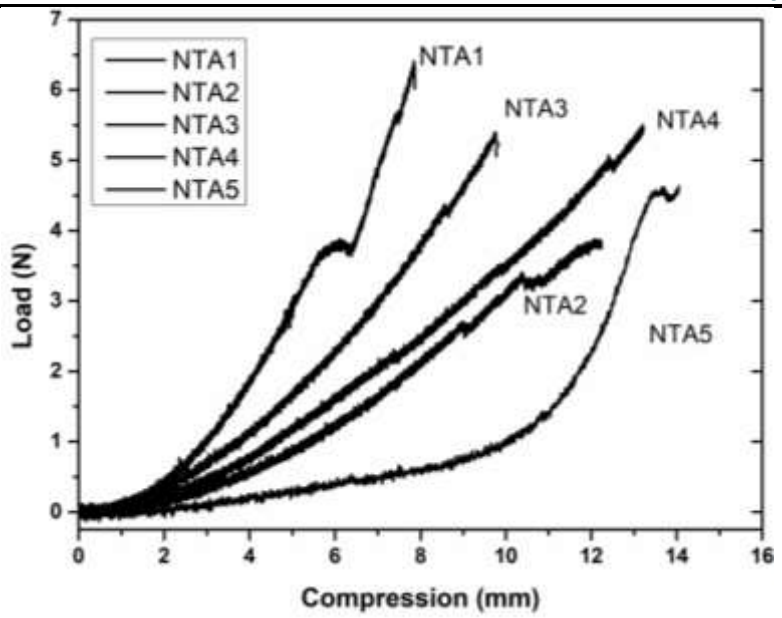

Figure 16: Plots of Load vs compression for NTA1, NTA2, NTA3, NTA4 and NTA5 copolymers

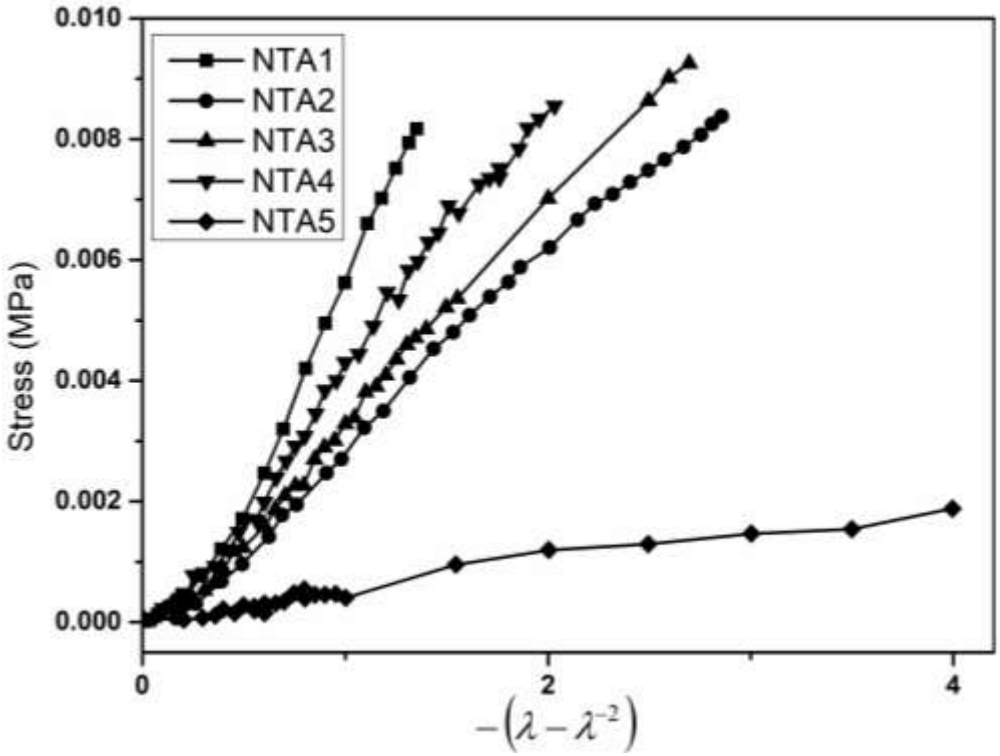

Figure 17: Plots of compression stress vs $-(\lambda - \lambda^{-2})$ for NTA1, NTA2, NTA3, NTA4 and NTA5 copolymers

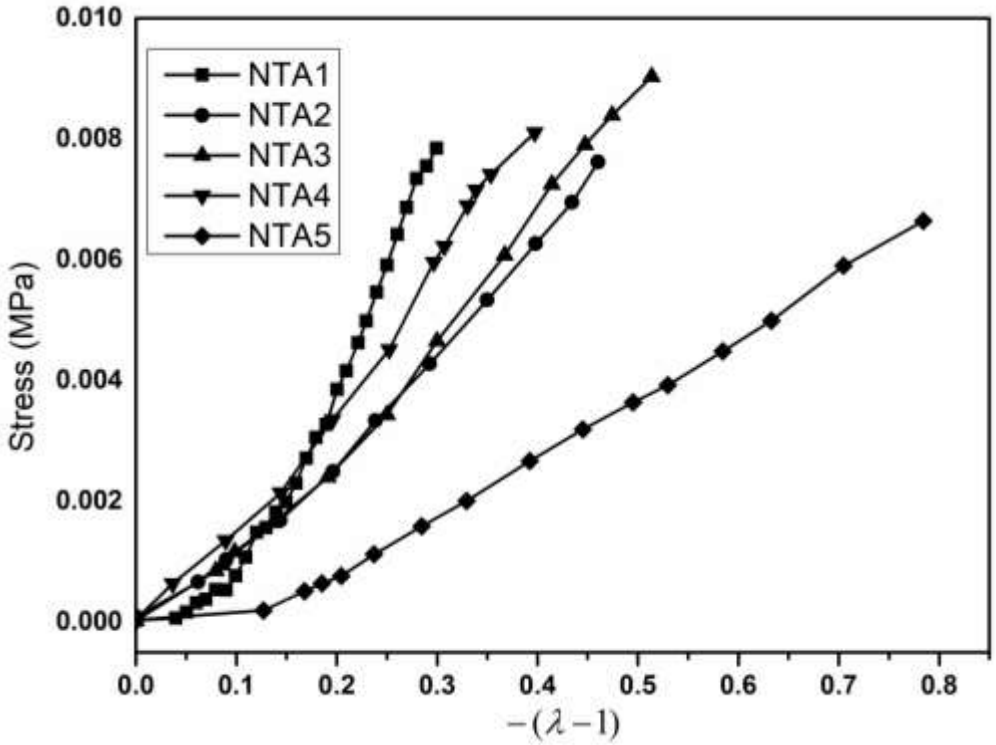

Figure 18: Plots of compression stress vs $-(\lambda - 1)$ for NTA1, NTA2, NTA3, NTA4 and NTA5 copolymers

Table 6 Elastic (E) and compression (G) modulus, for NTA1, NTA2, NTA3, NTA4 and NTA5 copolymers calculate by compression test

	Crosslinking ratio	E (modulus) MPa	G (Modulus) MPa	χ (at 25°C)
NTA1	1.6	0.0185	0.065	0.49
NTA2	4.8	0.0241	0.081	0.52
NTA3	19.4	0.107	0.101	0.57
NTA4	38.9	0.185	0.236	0.62
NTA5	58.4	0.298	0.424	0.69

3.8 Thermal Analysis

3.8.1 Thermogravimetric Analysis (TGA)

The thermal behavior of the copolymer hydrogels is illustrated in Figure 19. The thermogravimetric analysis (TGA) revealed a three-step weight loss profile. In the first stage, a mass loss of approximately 9.5% was observed between room temperature and 160°C, which can be attributed to the evaporation of physically entrapped water and/or water of crystallization associated with the polymer network. The second stage, occurring between 166°C and 326°C, corresponded to a weight loss of about 19%, arising primarily from the decomposition of side-chain functional groups. The major degradation step took place between 326°C and 700°C, with a mass loss of ~61%, which is attributed to main-chain scission accompanied by the release of carbon dioxide, water, nitrile compounds and imides (Shekhar et al., 2012a, 2012b, 2014, 2016, 2020, 2021).

These findings are consistent with previous reports by Van Dyke et al. (2018) and Martinez, Molina and Barbero (2018), who studied the thermal degradation of poly(acrylamide) homopolymers. Since the copolymers

studied here share a similar backbone structure, the overall degradation profile follows the same mechanism, with the primary distinction being the variation in crosslinking density. Notably, the concentration of crosslinking agent did not significantly influence the initial-stage degradation, a feature that is particularly important for practical applications where thermal stability at lower temperatures is critical.

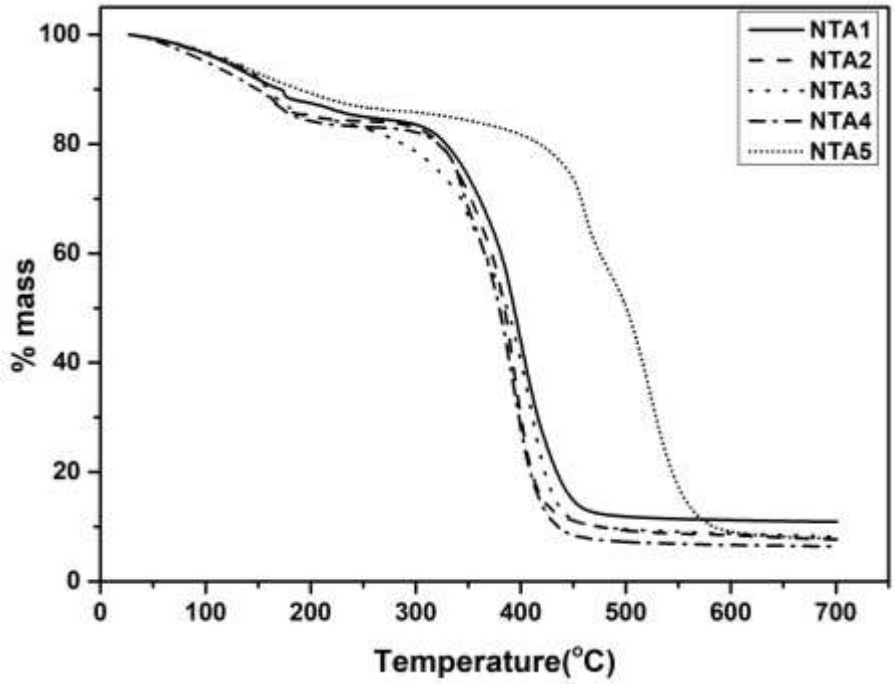

Figure 19: TGA Plots for NTA1, NTA2, NTA3, NTA4 and NTA5 Copolymers

3.8.2 Differential Scanning Calorimetry (DSC)

Figure 20 presents the DSC thermograms of NTA1, NTA2, NTA3, NTA4 and NTA5 hydrogels recorded in the temperature range of 27–700°C. An endothermic transition was observed around 164–196 °C, which can be attributed to the degradation of side-chain functional groups within the hydrogel matrices. In addition, two consecutive endothermic peaks, the first around 355°C and the second near 385°C, correspond to the main-chain decomposition of the crosslinked networks. These thermal events are accompanied by significant weight loss, consistent with the results of TGA analysis.

The glass transition temperatures (T_g) of the hydrogels were found to lie in the range of 170–200°C and showed a systematic increase with increasing crosslinking ratio. This behavior can be explained by the restricted mobility of polymer chains imparted by higher crosslinking density, which raises the T_g of the network. Furthermore, the broad transition observed in NTA5 indicates a wider distribution of molecular weights between crosslinks, reflecting structural heterogeneity at higher crosslinking levels.

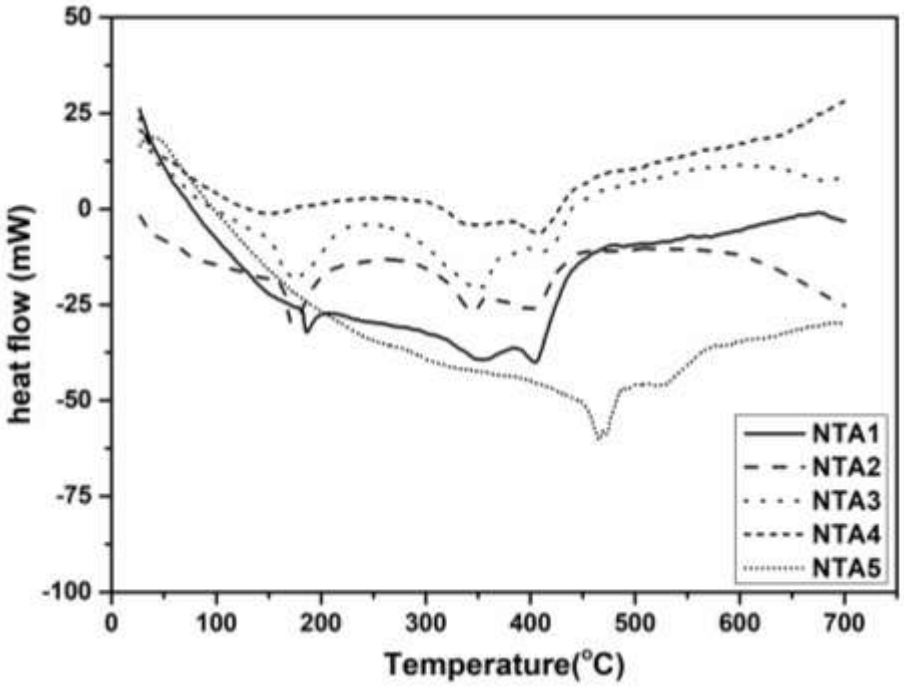

Figure 20: DSC Plots for NTA1, NTA2, NTA3, NTA4 and NTA5 copolymers

3.9 Conclusions

In this study, poly (NIPAM-co-NTBA-co-AAm) hydrogels were successfully synthesized by varying the relative amount of MBA as a crosslinker. The swelling capacity was found to increase with decreasing crosslinking ratio, while Flory–Rehner theory and equilibrium swelling experiments confirmed that the final crosslinking density increased with increasing crosslinking ratio. Furthermore, the molecular weight between crosslinks (M_c) decreased as the crosslinking ratio increased.

Compression measurements provided additional insights into the correlation between crosslinking ratio and the mechanical properties of the hydrogels. Both swelling and mechanical analyses consistently demonstrated a strong dependence of structural and functional properties on crosslinker content. The study of crosslinking density thus offered valuable understanding of swelling equilibria, network parameters and mechanical strength.

Overall our findings demonstrate that the crosslinked structure of poly (NIPAM-co-NTBA-co-AAm) hydrogels can be effectively tailored by varying the amount of MBA. Given their thermoresponsive nature and tunable properties, these hydrogels represent a versatile class of materials with potential applications in diverse fields. This work provides a foundation for correlating structure–property relationships in such systems, which is essential for optimizing synthesis protocols for targeted applications and possible industrial scale-up.

Acknowledgments: The authors are grateful to the Central Instrumentation Facility (CIF) at Birla Institute of Technology, Mesra, established in 2006 and the Technical Education Quality Improvement Programme (TEQIP) funded by World Bank for the State of the Art Instrumentation Facility.

Conflict of interest: There is no any conflict of interest to declare by the Authors.

References

1. Kamaliya B, Dave PN, Macwan PM (2022) Rheological investigations and swelling behaviour of hydrogels based on gum ghatti-cl-poly(N-isopropyl acrylamide-co-acrylicacid)/$CoFe_2O_4$ nanoparticles. Polymer Bulletin. https://doi.org/10.1007/s00289-004403-y

2. Jain A, Bajpai J, Bajpai AK et al (2020)Thermoresponsive cryogels of poly(2-hydroxyethyl methacrylate-*co*-*N*-isopropyl acrylamide) (P(HEMA-*co*-NIPAM)): fabrication, characterization and water sorption study. Polym. Bull. 77: 4417–4443.

3. Dharmasiri MB, Mudiyanselage TK (2021) Thermo-responsive poly(*N*-isopropyl acrylamide) hydrogel with increased response rate. Polymer Bulletin. 78:3183–3198

4. Xu X, Liu Y, Fu W, Yao M, Ding Z, Xuan J, Li D, Wang S, Xia Y, Meiwen Cao M (2020) Poly(N isopropylacrylamide)-Based Thermoresponsive Composite Hydrogels for Biomedical Applications. Polymers 12: 580.

5. Tang L,Wang L, Yang X, Feng Y, Lia Y, Feng W (2021) Poly(*N*-isopropylacrylamide)-based smart hydrogels: Design, properties and applications. Progress in Materials Science 115 : 100702.

6. Hamcerencu M, Desbrieres J, Popa M, Riess G 2020) Thermo-sensitive gellan maleate/*N*-isopropylacrylamide hydrogels: initial “in vitro” and “in vivo” evaluation as ocular inserts. Polymer Bulletin 77:741–755

7. Rafique N, Ahmad M, Minhas MU, Badshah SF, Malik NS, Khan KU (2021) Designing gelatin-based swellable hydrogels systemfor controlled delivery of salbutamol sulphate:characterization and toxicity evaluation. Polymer Bulletin 79:4535-4561.

8. Das S, Subuddhi U (2018) Guar gum–poly(*N*-isopropylacrylamide) smart hydrogels for sustained delivery of 5-fluorouracil. Polymer Bulletin.76:2945-2963.

9. Shekhar S, Mukherjee M, Sen AK (2020) Effect of surfactant on the swelling and mechanical behavior of NIPAM-based terpolymer. Polymer Bulletin 77:4355–4379

10. Shekhar S, Mukherjee M, Sen. AK (2021) Effect of Fe_2O_3 on the swelling, mechanical and thermal behaviour of NIPAM-based terpolymer. Polymer Bulletin. 78:5029–5054

11. Kousar F, Malana MA, Chughtai AH, Khan MS (2018) Synthesis and characterization of methacrylamideacrylicacid-N-isopropylacrylamide polymerichydrogel: degradation kinetics and rheological studies. Polym. Bulletin. 75:1275–1298

12. Paulin JA, Lopez-Aguilar JE, Fouconnier B, Vargas RO, Lopez-Serrano F(2022) Revisiting the Flory–Rehner equation: taking a closerlook at the Flory–Huggins interaction parameter and its functionality with temperature and concentrationwith NIPA as a case example. Polymer Bulletin 79:6709–6732

13. Saidi M, Dabbaghi A, Rahmani S, (2020) Swelling and drug delivery kinetics of click-synthesizedhydrogels based on various combinations of PEGand star-shaped PCL: influence of network parameterson swelling and release behavior. Polymer Bulletin 77:3989–4010

14. Shekhar S, Mukherjee M, Sen AK (2012) Synthesis, characterization and protein separation efficiency of N-isopropylacrylamide-co-N-tertiarybutylacrylamide-co-acrylamide-based hydrogel. Iran. Polym. J. 21(12): 895

15. Shekhar S, Mukherjee M, Sen AK (2012) Studies on thermal and swelling properties of Poly (NIPAM-co-2-HEA) based hydrogels. Advances in Materials Research. 1(4): 267-282

16. Shekhar S, Mukherjee M, Sen AK (2014) Synthesis and characterization of thermoresponsive terpolymer for protein separation. International journal of polymeric material and polymeric biomaterial. 63: 389-397

17. Shekhar S, Mukherjee M, Sen AK (2016) Swelling, thermal and mechanical properties of NIPAM based terpolymeric hydrogels. Polymer Bulletin 73(1): 125-145

18. Martinez MV, Molina M, Barbero CA (2018) Poly(N-isopropylacrylamide) CrosslinkedGels as Intrinsic Amphiphilic Materials. Swelling Properties Used to Build NovelInterphases. The Journal of Physical Chemistry B 122 (38): 9038–9048

19. Mah CH, Wu QY, Deen GR (2018) Effect of nature of chemical crosslinker on swellingand solubility parameter of a new stimuli-responsivecationic poly(N-acryloyl-N-propyl piperazine) hydrogel. Polym. Bull. 75**:**221–238

20. Zhang H, Huang X, Jiang J, Shang S, Song Z (2017)Hydrogels with high mechanical strength crosslinked by a rosin-based crosslinking agent RSC Adv. 7: 42541

21. Caykara T, Kiper S, Go¨khan Demirel (2006) Network Parameters and Volume Phase TransitionBehavior of Poly(*N*-isopropylacrylamide) Hydrogels. Journal of Applied Polymer Science. 101:1756–1762

22. Hoti G, Caldera F,Cecone C, Rubin Pedrazzo RA, Anceschi A, Appleton SL, Khazaei MY, Trotta F(2021) Effect of theCross-Linking Density on theSwelling and Rheological Behavior of Ester-Bridged _-CyclodextrinNanosponges. Materials. 14:478.

23. Salimi-Kenari H, Mollaie F, Dashtimoghadam E, Imani M, Nyström B (2018) Effects of chain length of the cross-linking agent on rheological and swelling characteristics of dextran hydrogels. Carbohydr. Polym. 181:141–149.

24. Jao WC, Chen HC, Lina CH, Yang MC (2009) The controlled release behavior and pH- andthermo-sensitivity of alginate/poly(vinylalcohol) blended hydrogels. Polym. Adv. Technol. 20: 680–688

25. Yildiz Y, Uyanik N, Erbil C (2006) Compressive Elastic Moduli of Poly(N-Isopropylacrylamide) Hydrogels Crosslinked with Poly(Dimethyl Siloxane)Journal of Macromolecular Sciencew, Part A: Pure and Applied Chemistry. 43:1091–1106

26. Bajpai SK, Singh S (2006) Analysis of swelling behavior ofpoly(methacrylamide-co-methacrylic acid) hydrogels andeffect of synthesis conditions on water uptake. Reactive & Functional Polymers. 66: 431–440

27. Gan LH, Deen GR, Gan YY, Tam KC (2001) Water sorption studies of new pH-responsive N-acryloyl-N'-methyl piprazine and methyl methacrylate hydrogels. Eur. Polym. J.37:1413-1478

28. Flory PJ (1953) Principles of Polymer Chemistry; Cornell University Press: Ithaca, NY, USA, 1953; ISBN 0801401348

29. Lopez CG, Richtering W (2017) Does Flory-Rehner theory quantitatively describe the swelling of thermoresposnive microgels. R. Soc.Chem.13:8271–8280.

30. Flory PJ, Rehner J (1943) Statistical Mechanics of Cross-Linked Polymer Networks II. Swelling. J. Chem. Phys.11:521–536.

31. Flory PJ, RehnerJ (1943) Statistical Mechanics of Cross-Linked Polymer Networks I. Rubberlike Elasticity. J. Chem. Phys.11:512-520.

32. Flory PJ, RehnerJ (1950) Statistical Mechanics of Swelling of Network Structures J. Chem. Phys.18:108-111

33. Xue W, Champ S, Huglin MB (2001) Network and swelling parameters of chemically crosslinkedthermoreversible hydrogels. Polymer 42:3665-3669

34. Jovanovic J, Adnadjevic B, (2007) Influence of poly(acrylic acid) xerogel structure on swelling kinetics in distilled water. Polym. Bull. 58:243-252

35. Flory PJ, Rehner J (1943) Statistical Theory of Chain Configuration and Physical Properties of High Polymers. Ann. N. Y. Acad. Sci. 44: 419–429

36. Valentín JL, Carretero-González J, Mora-BarrantesI, ChasséW, SaalwächterK (2008) Uncertainties in the determination of cross-link density by equilibrium swelling experiments in natural rubber. Macromolecules 41:4717–4729

37. Quesada-Pérez M, Maroto-Centeno JA, Forcada J, Hidalgo-Alvarez R (2011) Gel swelling theories: The classical formalism and recent approaches. Soft Matter 7:10536–10547.

38. Urich M, Denton AR (2016) Swelling, structure and phase stability of compressible microgels. R. Soc. Chem. 12: 9086–9094.

39. Fennell E, Huyghe JM (2019) Chemically Responsive Hydrogel Deformation Mechanics: A Review. Molecules 24:3521.

40. Castelli F, Pitarresi G, Giammona G (2000) Influence of different parameters on drug release from hydrogel systems to biomembrane model: evaluation by differential scanning calorimetry technique. Biomaterials 21:821-833.

41. Patras G, Qiao GG, Solomon DH (2001) Controlled Formation of Microheterogeneous Polymer Networks: Influence of Monomer Reactivity on Gel Structure. Macromolecules 34:6369-6401.

42. Berens AR, Hopfenberg HB (1978) Diffusion and relaxation inglassy polymer powders: 2. Separation of diffusion and relaxation parameters. Polymer 19:489–496

43. Ganji F, Farahani SV, Farahani EV (2010) Theoretical description of hydrogel swelling: A Review. Iran. Polym. J.19:375-398

44. Martínez-Vázquez N, del C Antonio-Cruz R, Alvarez-Castillo A, Mendoza Martinez AM, Morales-Cepeda AB, (2007) Swelling kinetics of hydrogels from methyl cellulose and poly (acrylamide). Revista Mexicana de ingeneeria quimica, 6 : 337-345

45. Thakur A, Wanchoo RK, Singh P (2011) Structural parameters and swelling behaviours of pH sensitive poly(acrylamide-co-acrylic acid) hydrogels. Chem. Biochem. Engg., 25:181-194

46. Enscore DJ, Hopfenberg HB, Stannett VT, Polymer (1977) Effect of particle size on the mechanism controlling n-hexane sorption in glassy polystyrene microspheres. 18:793-800.

47. Bajpai SK, Johnson S (2005) Superabsorbent hydrogels for removal of divalent toxic ions. Part I: Synthesis and swelling characterization / Reactive & Functional Polymers 62:271–283

48. Peppas NA, Brazel CS, (1999) Mechanisms of solute and drug transport in relaxing, swellable, hydrophilic glassy polymers. Polymer 40:3383-3398

49. Kardag E, Saraydin D (2002) Swelling of superabsorbent acrylamide-sodium acrylate hydrogels prepared using multifunctional crosslinkers. Turk. J. Chem.26: 863-875.

50. Peppas NA, Mikos AG, N.A. (1986) Hydrogels in Medicine and Pharmacy. CRC Press, BocaRaton FL 1:1–24.

51. Tanaka T, Fillmore DJ (1979) Kinetics of swelling of gels. J. Chem. Phys. 70:1214-1218

52. Erbil C, Yıldız Y, Uyanık N (2000) Effects of synthesis-solvent composition and initiator concentration on the swelling behaviour of poly(*N*-isopropylacrylamide) P(NIPAAM), poly(NIPAAM-*co*-dimethyl itaconate) and poly(NIPAAM-*co* itaconic acid) gels. Polym. Int. 49:795–800.

53. Erbila C, Topuza D, Gokceorena AT, Senkal BF, (2011) Network parameters of poly(N-isopropylacrylamide)/montmorillonite hydrogels: effects of accelerator and clay content Polym. Adv. Technol.22:1696–1704

54. Kabra BG, Gehrke SH (1991) Synthesis of fast response, temperature-sensitive poly(N-isopropylacrylamide) gel. Polym. Commun.32:322–323.

55. Matsuo ES, Orkisz M, Sun ST, Li Y, Tanaka T(1994) Origin of Structural Inhomogeneities in Polymer Gels. Macromolecules 27:6791–6796.